ELSEVIER

International Journal of Heat and Fluid Flow 20 (1999) 329–340

International Journal of HEAT AND FLUID FLOW

www.elsevier.com/locate/ijhff

# Transient analysis of Rayleigh–Bénard convection with a RANS model

S. Kenjereš, K. Hanjalić *

*Thermofluids Section, Department of Applied Physics, Delft University of Technology, Lorentzweg 1., PO Box 5046, 2600 GA, Delft, The Netherlands*

**Abstract**

Rayleigh–Bénard (RB) convection at high Rayleigh numbers was studied by transient Reynolds-averaged-Navier–Stokes (TRANS) approach. The aim of the study was to assess the RANS method in reproducing the coherent structure and large-scale unsteadiness in buoyancy-driven turbulent flows. The method can be regarded as a very large eddy simulation (VLES) combining the rationale of the LES and of RANS modelling. Following the experimental and DNS evidence that the RB convection is characterised by a coherent cellular motion with scales which are much larger than the scales of the rest of turbulent fluctuations, the instantaneous flow properties are decomposed into time-mean, periodic and random (triple decomposition). A conventional single-point closure (here an algebraic low-Re-number $k-\varepsilon-\overline{\theta^2}$ stress/flux model), used for the unresolved motion, was found to reproduce well the near-wall turbulent heat flux and wall heat transfer. The large scale motion, believed to be the major mode of heat and momentum transfer in the bulk central region, is fully resolved by time solutions. In contrast to LES, the contribution of both modes to the turbulent fluctuations are of the same order of magnitude. In the horizontal wall boundary layers the model accounts almost fully for the turbulence statistics, with a marginal contribution of resolved scales. The approach was assessed by comparison with the available direct numerical simulations (DNS) and experimental data using several criteria: visual observation of the large structure morphology, different structure identification techniques, and long-term averaged mean flow and turbulence properties. A visible similarity with large structures in DNS was observed. The mean flow variables, second-moments and wall heat transfer show good agreement with most DNS and experimental results for different flow cases considered. 

## 1. Introduction

Experiments and direct numerical simulations (DNS) show that Rayleigh–Bénard convection is characterised by large-scale coherent vortical structures. Its origin is in plumes and thermals that rise from the outer edge of the boundary layer on the heated surface (updrafts) and sink downward from the upper cold boundary (downdrafts). These large cellular structures (convection cells), found also in other convective layers heated from below, are regarded as the major heat and momentum carrier both in laminar and turbulent flows in the bulk of the central region. The rise and detachment of plumes (as well as their impingement on the opposing surface) cause a horizontal motion in the wall boundary layer, as found in the experiments by Chu and Goldstein (1973) and DNS of Cortese and Balachandar (1993). This motion is ultimately responsible for the wall heat transfer, as well as for the buoyancy, Siggia (1994). The latter, in turn, sustains the small-scale buoyant updraft at the edge of the boundary layer, which coalesce into large scale plumes. The morphology of these large structures differs in laminar and turbulent regimes and, particularly in the latter case, depends on the Rayleigh number (Ra). In the laminar regime the cells have a regular pattern with fixed locations of the thermal release. This regularity disappears with an increase in Ra number when the large structure becomes unsteady and more disorderly, with more persistent horizontal movement, although Chu and Goldstein (1973) detected some preferred locations of thermals release even in turbulent regime. An interesting question (particularly for statistical modelling) is whether in the turbulent regime this structure can still be regarded as a form of mean motion (with inherent unsteadiness), or whether it evolves at certain Ra number fully into turbulence (smooth spectrum and PDF) while retaining some coherence related to the flow geometry, (vertical dimension) and boundary conditions. Both, the experiments and DNS indicate that despite disorder, large coherent structures can be identified even at very high Ra numbers. Recent DNS by Kerr (1996) for of $\mathrm{Ra} \leqslant 2 \times 10^7$, which is close to the demarcation between the soft and hard turbulence regimes, Castaing et al. (1989), show that the large structures govern the apparent chaotic behaviour of turbulent RB convection. Beyond this value of Ra number DNS are not available and very little is known about the structure. Regularity and periodicity (except for fundamental mode with wave length associated with the flow height) have not yet been detected with any certainty. However, several sets of DNS results for low and moderate Ra numbers throw more light on the morphology of RB convection.

* Corresponding author. E-mail: hanjalic@duttwta.tn.tudelft.nl.

0142-727X/99/$ – see front matter 
PII: S0142-727X(99)00007-7

This brief qualitative overview provides a sufficient evidence of two distinct scales of motion: large amplitudes associated with plumes, thermals and convective cells, and the turbulence generated mainly in the wall boundary layer and carried away by the large scale structure. Whatever the nature of the large structure may be, it seems clear that its scale is well separated from the rest of turbulence, (which, depending on Ra number, may posses a complete spectrum of turbulence scales). This feature renders RB convection (and other turbulent flows with dominant large structures), suitable to single-point turbulence closures in unsteady (transient) computation. By fully resolving the large scale convective structure and associated momentum and heat transport (regarded as particularly difficult to model with single-point closures), a simple eddy-diffusivity – or algebraic closure can be used to model the unresolved motion. The only requirement is that the model should be capable of reproducing well the near wall statistical properties, the wall shear and heat transfer. This is the main difference as compared with subgrid models in the LES. The other difference is that the model accounts almost fully for the turbulence statistics in the near-wall region. This imposes a stricter requirement on the model of the unresolved motion as compared with a subgrid-scale model (SSG) in LES. However, a number of such models have been shown to satisfy these requirements, at least in simple wall parallel buoyancy driven flows. TRANS brings also a substantial computational advantage. The time step can be larger, allowing implicit time marching, the numerical mesh away from a solid boundary does not need to be very fine, and good statistics can be obtained with a relatively small number of realisations. The problem of defining inflow conditions at open boundaries is less restrictive. The method can be applied for much higher Ra numbers than it is possible with LES and can, therefore, be used for computations of complex flows of practical relevance.

This paper presents some results of application of the TRANS approach with an algebraic turbulence closure model to the computation of RB convection at high Ra numbers. The turbulence model includes the low-Re-number and wall proximity effects allowing integration up to the wall. The computed wall heat transfer, mean flow properties and second-moments are compared with available experimental data, DNS, as well as with results of two-dimensional steady RANS calculations. The transient realisations are analysed using the criteria from the critical point theory for the identification of the coherent structure, its spatial organisation and its role in RB convection at high Rayleigh numbers.

## 2. Governing equations, model and numerical method

The momentum and energy equation for the instantaneous motion can be written as

$$\frac{\partial \hat{U}_i}{\partial t} = \frac{\partial}{\partial x_j}\left(\nu\frac{\partial \hat{U}_i}{\partial x_j} - \hat{U}_i\hat{U}_j\right) + \beta g_i(\hat{T} - T_{\mathrm{ref}}) - \frac{1}{\rho} \times \frac{\partial(\hat{P} - P_{\mathrm{ref}})}{\partial x_i}, \tag{1}$$

$$\frac{\partial \hat{T}}{\partial t} = \frac{\partial}{\partial x_j}\left(\alpha\frac{\partial \hat{T}}{\partial x_j} - \hat{T}\hat{U}_j\right). \tag{2}$$

For flows with a distinct large structure, any instantaneous fluid property at a point $\hat{\Phi}(x_i,t)$ can be decomposed into the time-mean $\overline{\Phi}(x_i)$, periodic $\tilde{\Phi}(x_i,t)$ and random $\phi(x_i,t)$, i.e.

$$\hat{\Phi}(x_i,t) = \overline{\Phi}(x_i) + \tilde{\Phi}(x_i,t) + \phi(x_i,t). \tag{3}$$

The long-term averaged second-moments of the instantaneous variables contain the cross terms, in addition to the second-moments of each the periodic and random motion. For a general case of a turbulence with a continuous spectrum, the cross terms must be provided, or modelled jointly with the second-moments of the random motion. In the present case we assume that the periodic and random motions have very different scales and expect that these motions do not interact directly, so that the cross terms can be neglected. With this assumption, the long-term averaged energy equation reduces to

$$\frac{\partial}{\partial x_j}\left(\alpha\frac{\partial \overline{T}}{\partial x_j} - \overline{TU_j} - \overline{\tilde{T}\tilde{U}_j} - \overline{\theta u_j}\right) = 0. \tag{4}$$

The first three terms are provided from TRANS and the last term from the single-point model. Further averaging over homogeneous (horizontal) planes yields the expression for the total heat flux in the vertical direction ($z$):

$$\alpha\frac{\partial \overline{T}}{\partial z} - \overline{\tilde{T}\tilde{W}} - \overline{\theta w} = \frac{q_w}{\rho c_p} = \mathrm{const.} \tag{5}$$

The contribution of the unresolved motion to the heat flux $-\overline{\theta u_j}$ is modelled by a 'reduced' algebraic flux/stress model, Hanjalić (1994); Kenjereš and Hanjalić (1995). This model is derived from the modelled differential transport equation for $\overline{\theta u_i}$ by assuming weak equilibrium, but retaining all major flux production terms

$$\overline{\theta u_i} = -C\frac{k}{\varepsilon}\left(\overline{u_i u_j}\frac{\partial \tilde{T}}{\partial x_j} + \xi\overline{\theta u_j}\frac{\partial \tilde{U}_i}{\partial x_j} + \eta\beta g_i\overline{\theta^2}\right). \tag{6}$$

The stresses are also supplied from similar algebraic truncation of the full transport equations. The algebraic expressions are closed by solving the transport equations (modified for low-Re-number and near-wall effects) for the turbulence kinetic energy $k$, its dissipation rate $\varepsilon$ and for temperature variance $\theta^2$, resulting in a three-equation model $k-\varepsilon-\theta^2$. This model was earlier applied to steady RANS computation of a variety of buoyancy driven flows and was found to reproduce well the major mean flow properties, turbulent and wall heat flux in most of the cases considered, Hanjalić (1994), Kenjereš and Hanjalić (1995) and Dol et al. (1997). It is noted, that the second-moment statistics are obtained as a sum of resolved and unresolved (modelled) contributions, as follows from the long-term averaging, e.g. for variables $\Phi$ and $\Psi$:

$$\overline{\hat{\Phi}\hat{\Psi}} - \overline{\Phi}\overline{\Psi} = \overline{\tilde{\Phi}\tilde{\Psi}} + \overline{\phi\psi}. \tag{7}$$

In contrast to LES, both contributions are usually of the same order of magnitude and close to a wall the unresolved part is often larger, as is the case of the turbulent heat flux and temperature variance (see later).

Numerical simulation were performed by a fully vectorised version of finite volume Navier–Stokes solver for three-dimensional flows in structured non-orthogonal geometries, with Cartesian vector and tensor components and collocated variable arrangement. The SIMPLE algorithm was used for the treatment of the pressure–velocity coupling. The second order accurate central difference scheme (CDS) was applied for the discretisation of the diffusive terms and second order linear-upwind scheme (LUDS) for the convective terms. The time marching is performed by a fully implicit second order three-time-level method which allows larger time steps to be used. In view of the fact that only large scales are being resolved, the use of an implicit time-marching seems both justified and rational. Typical computations covered 150–300 nondimensional time units $\tau^* = \tau\sqrt{\beta g \Delta T H}/H$ which correspond roughly to 10–20 convective time scales based on

convective velocity and characteristic cell circumference, Kerr (1996).

## 3. Long-term averaged properties

In order to compare the adopted approach with DNS and LES data and with results of the earlier steady 2D RANS computations, a series of time-dependent simulations of Rayleigh–Bénard convection were performed. Considered were different configurations and different values of Ra number: the case with a horizontal flat wall at $Ra = 10^7$, for which two different aspect ratios were considered (4:4:1 and 8:8:1) with the grid of $62^3$ and $122^2 \times 62$ CV respectively, and $Ra = 10^9$ with (4:4:1 aspect ratio and grid size of $82^3$ CV).

For the lower Rayleigh number considered the configurations were chosen to correspond closely to those for which DNS were previously performed by Grötzbach (1982), Cortese and Balachandar (1993), Wörner (1994), Kerr (1996). The LES reported by Eidson (1985) and Wong and Lilly (1994) were also performed for similar situations and Ra numbers. Computations were also performed for a larger value of Ra number ($10^9$) in order to demonstrate applicability of TRANS in range of high Ra numbers where the application of DNS techniques will require an enormous amount of computational resources, as shown by Grötzbach (1983) and Kerr (1996).

### 3.1. Integral heat transfer characteristics

The first step in validation of the proposed turbulent closure model for thermal field is to make comparison of the integral Nusselt number. We compare our results with several experimental, DNS and LES studies for different values of Ra number. First, the performance of 3D TRANS was compared with previously calculated 2D RANS results, which were performed for a wide range of Ra numbers from $10^6$ up to $10^{12}$, and for different aspect ratios, as well as using different closure levels in modelling of the turbulent heat flux, Kenjereš and Hanjalić (1995). As seen in Fig. 1, the 2D steady RANS and 3D TRANS, with the same algebraic flux/stress model, yield almost identical Nusselt numbers, both for $Ra = 10^7$ and $Ra = 10^9$.

Next we compare the 3D TRANS results in a range of low and moderate Ra numbers with the DNS results of Kerr (1996) and with two different sets of LES, reported by Eidson (1985) and Wong and Lilly (1994). In addition, the experimental correlations proposed by Chu and Goldstein (1973), Fitzjarrald (1976), Threlfall (1975) and Wu and Libchaber (1992) are also plotted, Fig. 1. The LES of Eidson (1985) yielded the values of $Nu = 8$, 9.5, 12.5, 13.8, 18 and 19 for $Ra = 3.75 \times 10^5$, $6 \times 10^5$, $1.5 \times 10^6$, $2.5 \times 10^6$, $10^7$ and $10^8$, respectively, which are much different from the DNS and experimental correlations. For lower Ra numbers up to $2.5 \times 10^6$, LES seriously over-predicts Nu number (by more than 40%). According to Eidson (1985), this Ra value was the highest for which the simulatations were successful. For higher values of Ra number LES gave anomalous results, which Eidson attributed to insufficient resolution. It is interesting to note that for $Ra = 10^8$ Eidson (1985) obtained an almost identical Nu number as we obtained by 2D RANS with the standard isotropic eddy diffusivity hypothesis, denoted in Fig. 1 as SGDH ('simple gradient diffusion hypothesis'). However, this model was found inadequate for modelling buoyancy driven flows because it presumes a full alignment between the components of the turbulent heat flux and mean temperature gradient, Ince and Launder (1989), but also because it does not account for the direct buoyancy effects on the heat flux (the third term in Eq. (6), Hanjalić (1994). This leads to a delayed effect of Ra number and produces laminar-like solutions at relatively high Ra numbers. Not accounting for buoyancy in the SGS model may be the reason for the failure of LES at higher Ra numbers: Eidson (1985) used the simple Smagorinsky subgrid model, which is akin to the isotropic eddy diffusivity model in RANS. However, more recently Wong and Lilly (1994) discussed the inclusion of the buoyancy effects into SGS model. They proposed a modification and performed LES with two slightly different dynamic SGS models, which resulted in a small difference. Unfortunately, they reported simulations for only one value of $Ra = 3.8 \times 10^5$. The computed Nu number for this Ra number was even higher than that of Eidson (1985). Peng and Davidson (1998) obtained similar Nusselt numbers, despite the modifications for buoyancy effects in their SGS. This consistent overprediction of Nu number by LES in comparison with Kerr (1996) DNS data and experimental correlations show that despite the introduction of buoyancy effect into SGS, LES has difficulties in reproducing the near-wall and wall properties.

### 3.2. Mean temperature, its gradient and temperature variance

The computed long-term and spatially averaged mean temperature and temperature variance for various values of Ra are shown in Figs. 2 and 3, respectively. The 2D RANS profiles were obtained by cell averaging in order to eliminate the effects of the side boundaries, while 3D TRANS and DNS profiles were obtained by spatial averaging over the entire horizontal planes. As seen in Fig. 2(a), the mean temperature profiles compared by 3D TRANS and 2D RANS methods agree very well with the DNS results over the entire cavity height. Even in the near wall region, both simulations show very good agreement with the DNS, with somewhat better results obtained by 3D TRANS as the distance from the wall increases. This is clearly demonstrated in the semi-logarithmic plot in Fig. 2(b), where the temperature is scaled with buoyancy velocity and derived buoyancy temperature, showing a full near-wall similarity of profiles for a range of Ra numbers and excellent agreement with DNS.

The mean temperature profile exhibits a characteristic distribution with a very steep gradient in the near-wall region and almost isothermal core region. This behaviour of the mean temperature explains why a very fine grid resolution is needed for DNS at high Ra numbers, as argued by Grötzbach (1983). On the other hand, the existence of almost isothermal core region clearly shows that simple gradient models for the turbulent heat flux are inappropriate for configurations with heating from below.

The temperature variance is much more difficult to reproduce than the mean temperature. With an increase in the Rayleigh number the peak moves from the centre closer to the wall indicating a thinning of the thermal boundary layer, Fig. 3. Note two contributions to the total variance (Eq. (7): $\overline{\tilde{T}^2} = \overline{\hat{T}^2} - \overline{T}^2$ from the large scales (full resolution) and from the model $\overline{\theta^2}$ of the unresolved motion (obtained from the transport equation for $\overline{\theta^2}$). The total variance is denoted in Fig. 3 by 'T' and the model contribution by 'M'. As seen, good agreement is obtained in comparison with a DNS profile at $Ra = 10^7$. The profiles of temperature variance obtained by 3D TRANS show an improvement in the prediction of the peak values in the near-wall region as well as in the central part of the cavity as compared with 2D RANS computations (for which only the modelled part is shown). When normalized with buoyancy temperature the TRANS computations fall

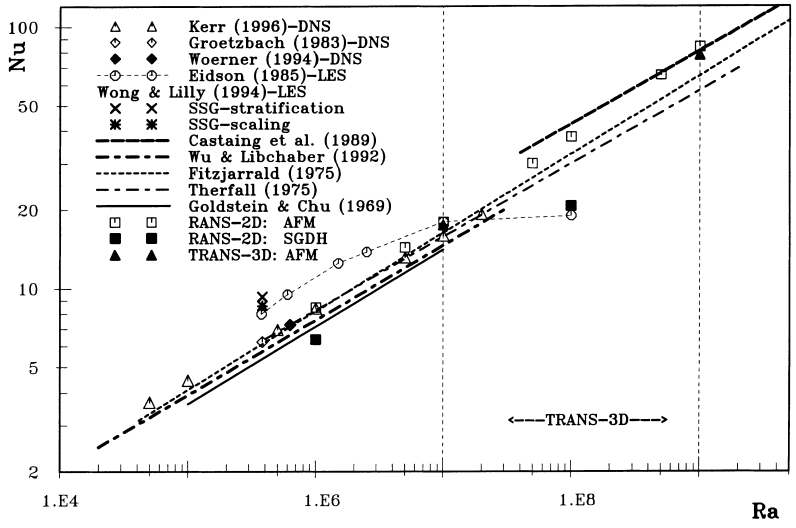


Fig. 1. Comparison of the calculated integral Nusselt numbers with experimental correlations, DNS and LES results.

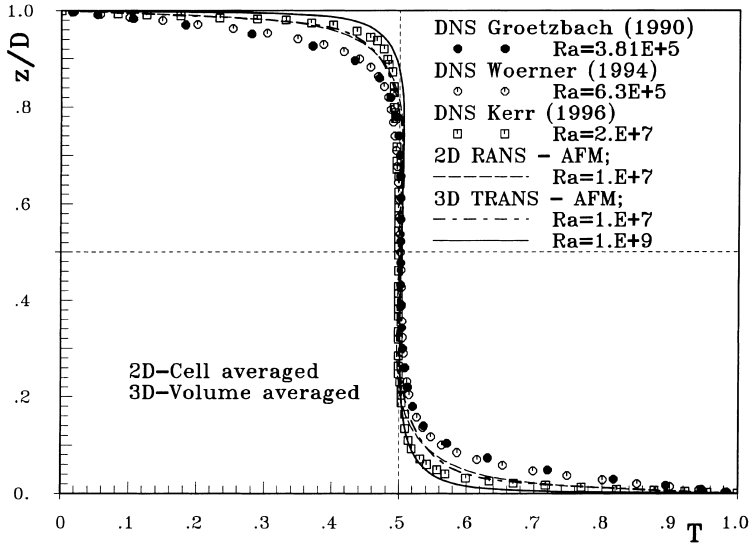


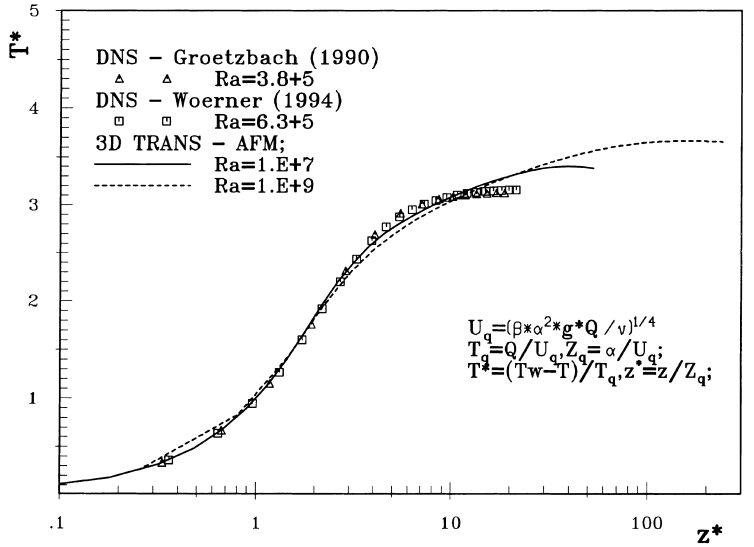


Fig. 2. (a) Long-term averaged temperature distribution in RB convection for different Ra numbers; (b) scaling of mean temperature profiles, TRANS and DNS.

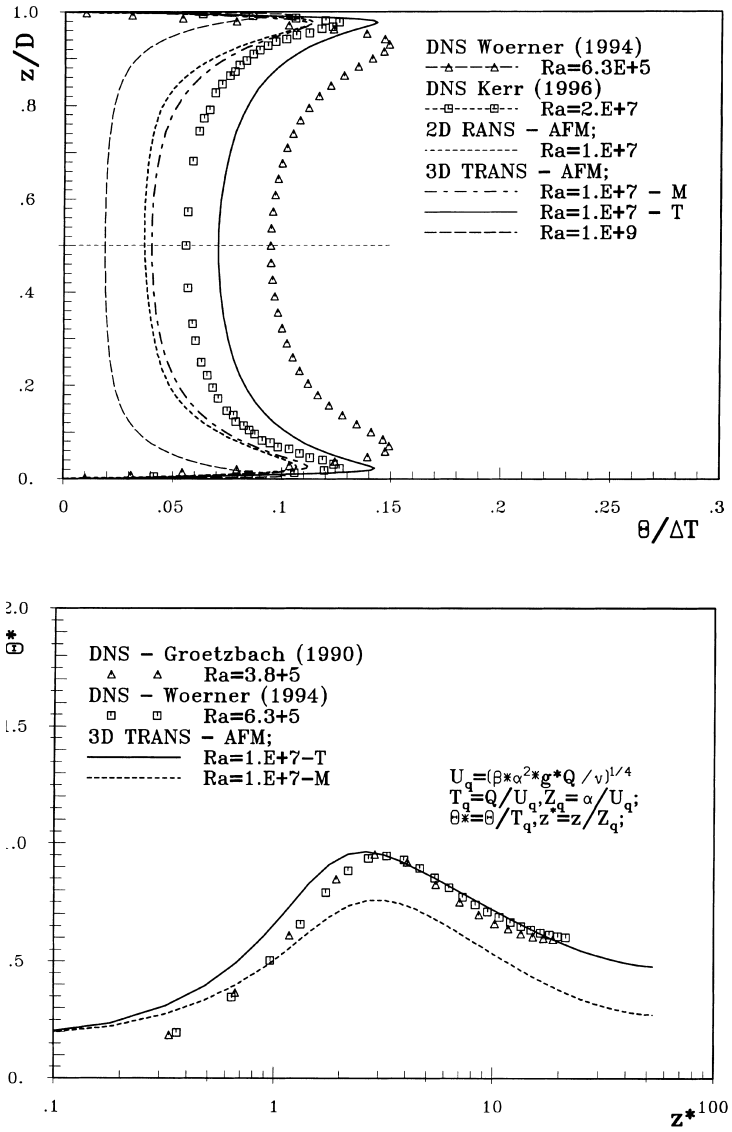


Fig. 3. (a) Temperature variance profiles in RB convection for different values of Ra number: M – modelled, T – total; (b) scaling of temperature variance profiles, TRANS and DNS.

almost on the same curve as DNS results, despite a difference in Ra numbers, Fig. 3(b).

Fig. 4 shows the two contributions to the turbulent heat flux and temperature variance (squared). As indicated in the introduction, both contributions are of the same order of magnitude, with the modelled one prevailing in the near-wall region. The sum of all three contributions to the total heat flux (Eq. (5)), normalised with the wall heat flux, shows that the long-term averaged total heat flux is indeed constant over the entire channel cross-section, as it should be, whereas most DNS and, in particular, LES show a substantial variation due to incomplete resolution. A good modelling of the near wall heat flux and temperature variance is a prerequisite for accurate reproduction of the wall Nu number, which agrees well with the available DNS and experimental correlations (Fig. 1), as discussed earlier.

The mean temperature gradient in RB convection has been the subject of several studies, aimed at establishing the power scaling laws in different regions. Despite substantial experimental and DNS evidence, the power law at high Ra numbers is still controversial. Two different laws were proposed based on theoretical and similarity considerations. Based on the assumption that the only relevant length scale is the actual distance from the wall, Priestley (1955) stated that the vertical gradient of the mean temperature obeys a $-4/3$ law. In contrast, Malkus (1954) argued that the thermal boundary layer thickness is the characteristic length scale. Together with the assumption that the non-dimensional heat flux is a linear function of this length scale, Malkus arrived to a $-2$ law. It is interesting to note that most experimental studies confirmed the existence of $-2$ power law and only a few suggest a possibility of $-4/3$ slope. Adrian et al. (1986) proposed and experimentally verified a unified multi-layer theory which actually includes both previously mentioned power laws. These authors indicated at two possible reasons for the failure in observing of a $-4/3$ law in previously performed experimental studies: the measurements reported did not extend far enough from the wall, or the Ra was not large enough. Of course, numerical simulations can provide a detailed insight in the behaviour of the mean temperature

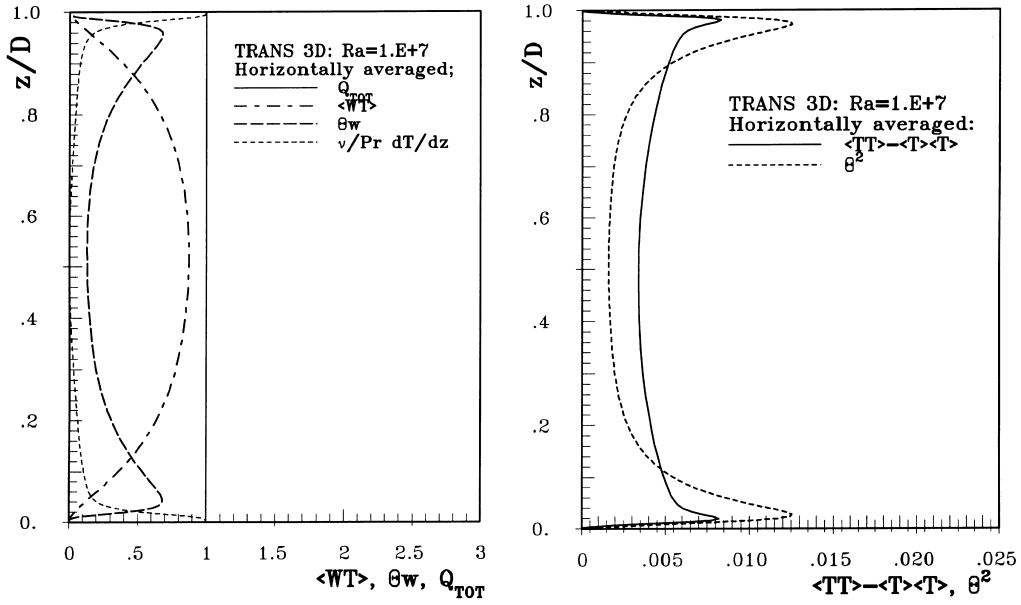


Fig. 4. The modelled and resolved parts of: (a) vertical turbulent heat flux; (b) temperature variance.

gradient. Unfortunately, the high Ra number range is far beyond the DNS limits (up to $2 \times 10^7$ in 1998) so that DNS at present cannot provide possible clarification. Contrary to current DNS limitations, TRANS technique can be easily extended to much higher Ra, ($\mathrm{Ra} = 10^{12}$ was easily computed), with only a moderate computational costs. To demonstrate that, the calculations at $\mathrm{Ra} = 10^9$ as a representative of high Ra number range were performed, Fig. 5. It is interesting to note that both 2D RANS and 3D TRANS equipped with AFM model correctly reproduce the mean temperature gradients which is in excellent agreement with the physical model of Adrian et al. (1986) and Chung et al. (1992). Three distinctive power regions are very well reproduced: a conductive region with a constant mean temperature gradient for $0 \leqslant z^* \leqslant 1$, a transitional region with a $-2$ law up to $z^* \approx 5$ and, finally, a convective region which obeys a $-4/3$ power law for $z^* > 5$.

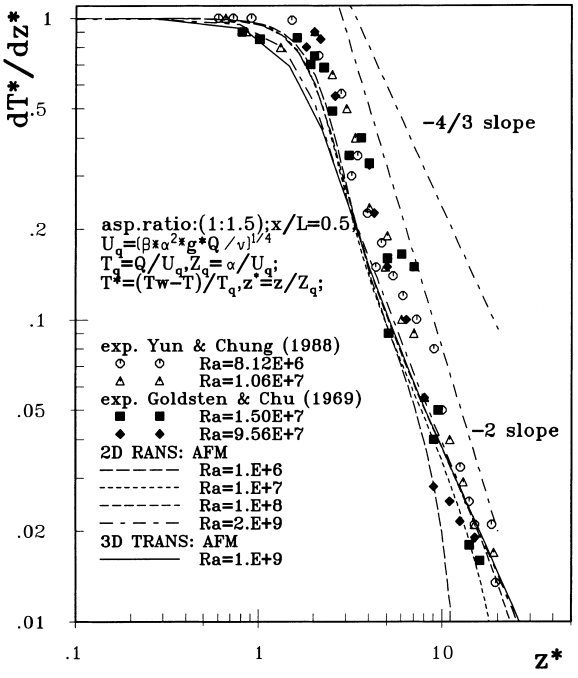


Fig. 5. Dimensionless mean temperature gradient.

## 4. Identification of large structures

The most common definition of coherent structures is associated with vortical motion. However, different possibilities for identification of vortex cores as representatives of a vortical motion have been proposed. Various definitions of a vortex can also be in the literature. The most frequently cited definition is the one proposed by Robinson (1991): "A vortex exists when instantaneous streamlines mapped onto a plane normal to the vortex core exhibit a roughly circular or spiral pattern, when viewed from a reference frame moving with the centre of the vortex core". But the streamlines representation of velocity fields requires a significant amount of CPU time for their calculations and very often the final output cannot bring a clear picture of the flow, especially in complex situations. The clarity can be improved by plotting two-dimensional streamlines projections onto a characteristic plane, but problem of high computational costs still remains. In order to avoid extensive calculations, the introduction of some representative scalar quantities is needed. Robinson (1991) proposed low-pressure regions as regions which are expected to correspond well to the vortex cores. By analysing the late stage of transition in a channel flow, Sandham and Kleiser (1992) confirmed that the same method represents well coherent structures. Kasagi et al. (1995), adopted the same approach in analysing their DNS database of the channel flow.By plotting the instantaneous vectors in various sections, and found that many of low-pressure regions correspond to the rotational fluid motions. But low-pressure regions can misrepresent the vortex core due to non-local character of the pressure which may have a larger scale than the vortex core, as shown by Jeong and Hussain (1995). The next scalar parameter which has been often used for the identification of the flow topology is the modulus of vorti-

city: $|\omega_i| = |\varepsilon_{ijk}\partial U_j/\partial x_k|$. This approach was successful in free-shear flows, Jeong and Hussain (1995), but problems persists in the near-wall regions where the vorticity magnitude shows a maximum value (regions where maximal velocity gradients naturally occur). However, the high vorticity in the near wall region originates from shear and not from a swirling or rotational motion. This leads to a conclusion that $|\omega_i|$ is not a suitable parameter for vortex identification in RB convection.

A method of critical points (defined as positions where the streamlines slope is indeterminate and the velocity is zero) was introduced in Perry and Chong (1987) in order to assess the flow pattern at each point of the flow. According to this theory, the eigenvectors and eigenvalues of the mean velocity gradient tensor ($A_{ij}=\partial U_i/\partial x_j$) evaluated at a critical point define the flow pattern. The eigenvalues and eigenvectors of the velocity gradient tensor ($A_{ij}$) are obtained by solving the characteristic equation, $\lambda^3 - I_1\lambda^2 + I_2\lambda - I_3 = 0$, where

$$I_1 = \frac{\partial U_i}{\partial x_i}, \quad I_2 = -\frac{1}{2}\frac{\partial U_i}{\partial x_j}\frac{\partial U_j}{\partial x_i}, \quad I_3 = \mathrm{Det}(A_{ij}) \tag{8}$$

are three invariants of ($A_{ij}$) and for incompressible flows $I_1 = 0$.

A definition of vortex core as a region with complex eigenvalues of ($A_{ij}$) was proposed by Chong et al. (1990), implying that the local streamline pattern is closed or spiral in a reference frame moving with the point of interest. The discriminant of the characteristic equation can be written as

$$\Delta = \left(\frac{1}{3}I_2\right)^3 + \left(\frac{1}{2}I_3\right)^2. \tag{9}$$

This determines the nature of the eigenvalues of $A_{ij}$ as follows: $\Delta > 0$ gives one real and two conjugate-complex eigenvalues, $\Delta < 0$ gives three real distinct values and finally, $\Delta = 0$ gives three real values of which two are equal. A map of all possible solutions of characteristic equations can be

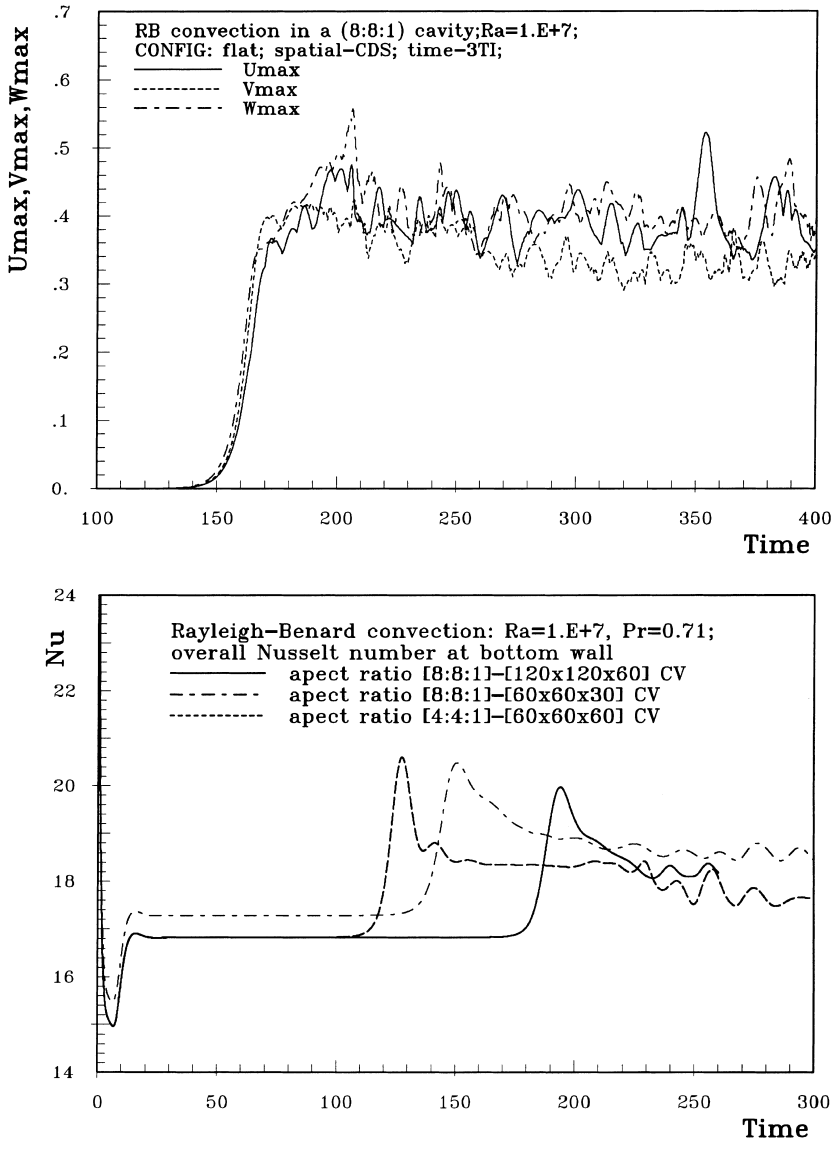


Fig. 6. Time evolution of maximum velocity components and overall Nusselt numbers at bottom hot wall for two different aspect ratios, Ra = $10^7$.

created by plotting trajectories of constant discriminant $\Delta$ in $I_2 - I_3$ plane. From the definition of the discriminant of the characteristic equation it follows that the complex eigenvalues occur when $\Delta > 0$. Recently, Chong et al. (1998) applied their "$\Delta$" approach to analyse the structure of wall-bounded shear flows including boundary layers with zero-pressure-gradient, separation and reattachment. They found that a positive small value of the discriminant identifies very well vortical regions.

The definition of eddy structure as a region with positive second invariant $I_2$ of the velocity gradient tensor $A_{ij}$ was introduced in Hunt et al. (1988) and Blackburn et al. (1996). The second invariant $I_2$, (denoted in figures as Q in accord with notation of Hunt et al. (1988) can be interpreted as a measure of the relative importance of the shear strain $S_{ij} = 0.5(\partial U_i/\partial x_j + \partial U_j/\partial x_i)$ and the rotation rate $\Omega_{ij} = 0.5(\partial U_i/\partial x_j - \partial U_j/\partial x_i)$. In regions where $I_2$ is positive, the rotational rate prevails over shear strain rate and where $I_2$ is negative, the reverse is true.

A kinematic vorticity number $\mathcal{N}_k$ was used in Melander and Hussain (1992) as a measure of the quality of rotation, defined as

$$\mathcal{N}_k = \left( \frac{|\omega_i|^2}{2S_{ij}S_{ij}} \right)^{1/2}. \tag{10}$$

When $\mathcal{N}_k = 0$, the irotational motion is present and in the case $\mathcal{N}_k = \infty$, the motion has a character of a solid-body rotation.

In the present identification of the large coherent structures in RB convection, we analyse in parallel one realisation of DNS and several realisations of TRANS, using three different criteria: $\Delta$, $I_2$ and $\mathcal{N}_k$.

### 4.1. Low Ra number

The analysis of the flow structure for TRANS simulations at $\mathrm{Ra} = 10^7$ and a direct comparison with DNS results of Wörner (1994) for $\mathrm{Ra} = 6.3 \times 10^5$ will be first presented. In order to portray the dynamic behaviour of the flow, the characteristic time evolution of the maximum velocity components, as well as the overall Nusselt number at the hot wall, are monitored for two different aspect ratios, Fig. 6. Three characteristic time periods can be distinguished: The conduction dominated period which takes place in the initial stage of heating, the transitional period and fully turbulent convective

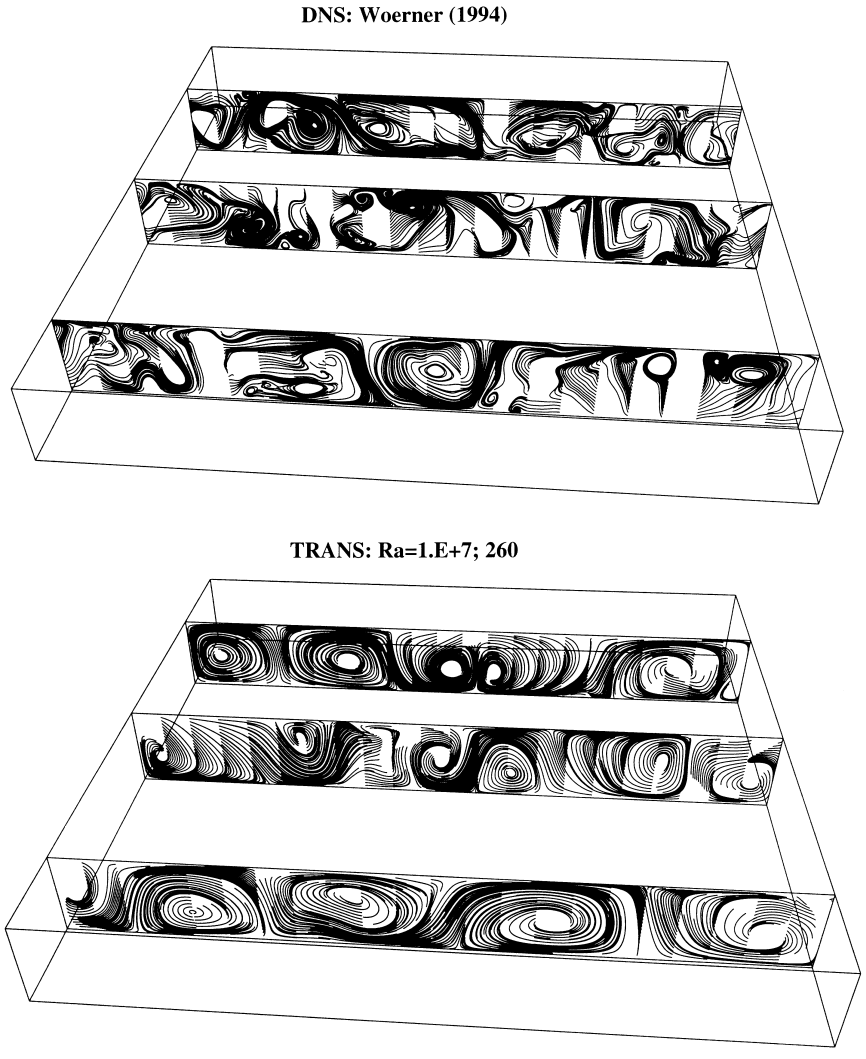


Fig. 7. Instanteneous trajectories of massless particles in the central horizontal plane for one DNS ($\mathrm{Ra} = 6.5 \times 10^5$) and one TRANS realisation ($\mathrm{Ra} = 10^7$).

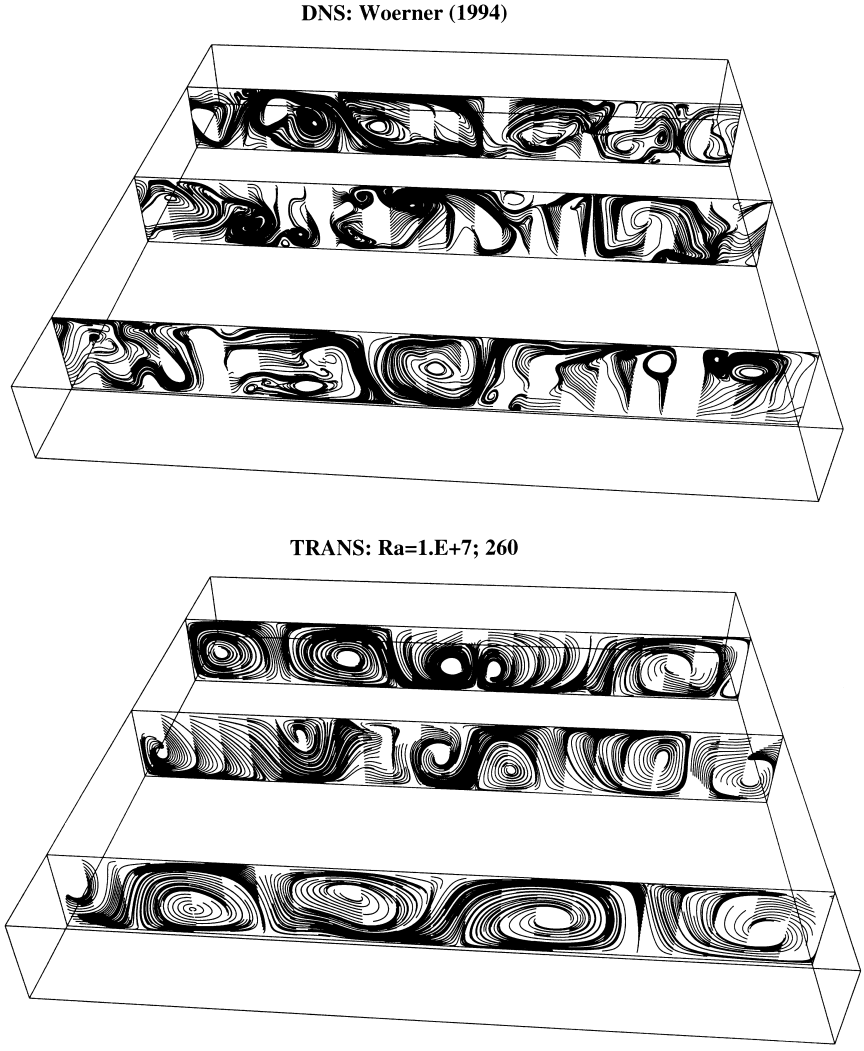


Fig. 8. Instanteneous trajectories of massless particles in three vertical planes for one DNS ($Ra = 6.5 \times 10^5$) and one TRANS realisation ($Ra = 10^7$).

period. The two different aspect ratios show a very similar behaviour of the Nusselt numbers. The main difference is in the position where intensive heat transfer occurs, $\tau^* = 110$ for [4:4:1] and $\tau^* = 180$ for [8:8:1], where $\tau^* = \tau\sqrt{\beta g \Delta T H}/H$. As seen, the lower aspect ratio promotes turbulent regime earlier. In order to obtain a better insight in the flow structure and to

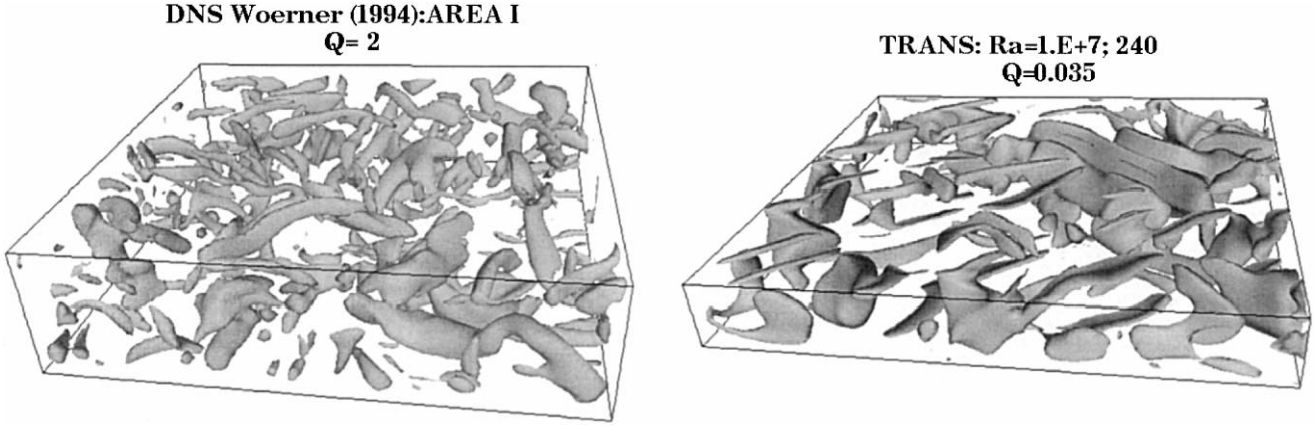


Fig. 9. Comparison of vortical structures in DNS ($Ra = 6.3 \times 10^5$) and TRANS ($Ra = 10^7$) for different values of the second invariant of the velocity gradient tensor ($I_2 = Q$).

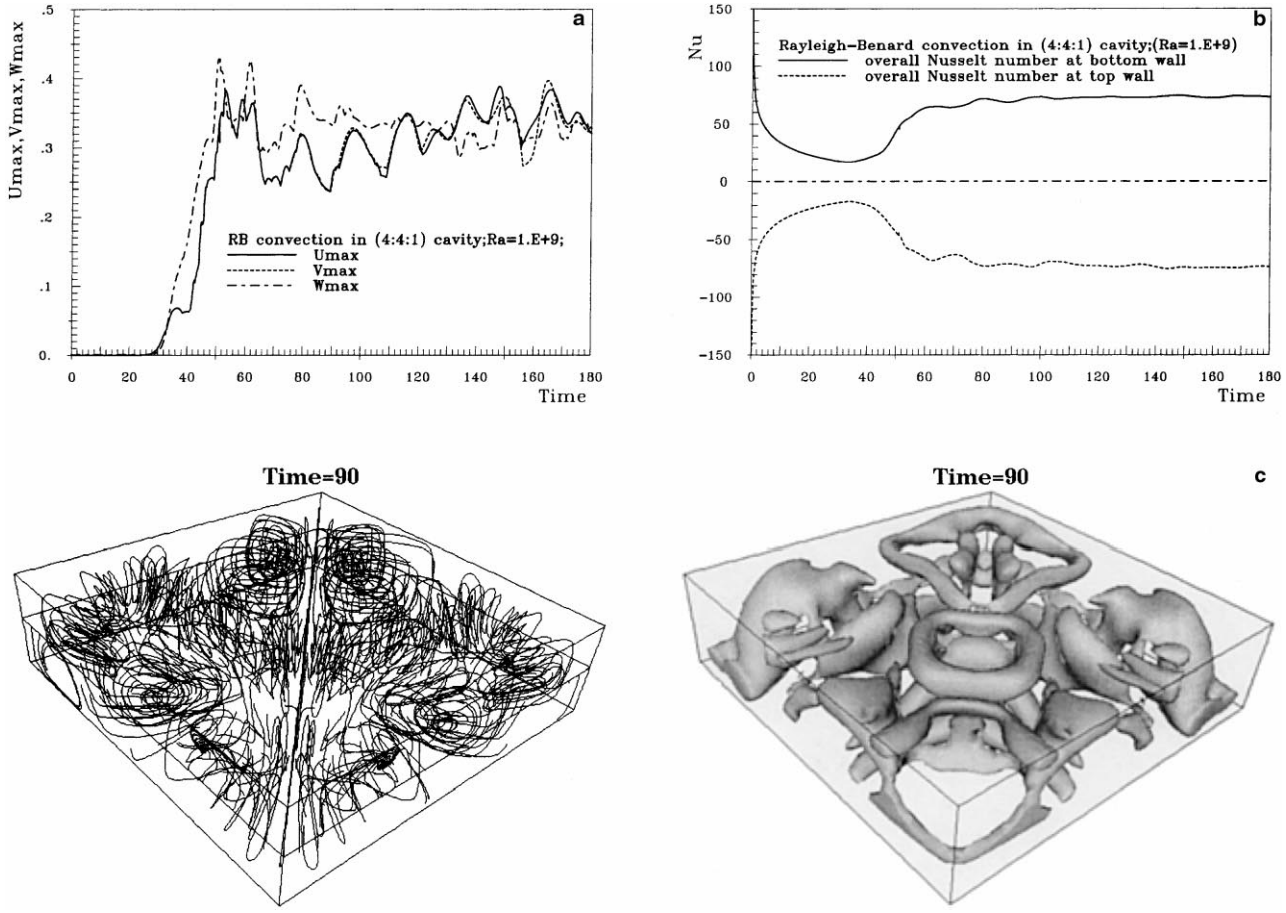


Fig. 10. (a) Time evolution of the maximum velocity components; (b)Time evolution of integral surface *Nu* number; (c) Instantaneous streamlines and the second invariants of the velocity gradient tensor, $I_2$ for one TRANS realisation at $\mathrm{Ra} = 10^9$ for the flat wall.

compare how TRANS instantaneous fields correspond to Wörner's DNS data, the streamlines distribution in the central horizontal plane, $z^* = 0.5$ and in three vertical planes, $y^* = 0.15, 0.5, 0.85$ were plotted for one DNS realisation and for one instantaneous TRANS field, Figs. 7 and 8. The streamlines are plotted by releasing 1500 massless particles from uniformly distributed origins over the sampling planes of the instantaneous fields, and their distributions were calculated by applying a second order Runge-Kutta time advection method. Although the streamline pictures portray very complex flow, three distinctive regimes can be observed: the regions with a strong and well defined plane circulation (roll structure), the regions with one-dimensional movements (dark lines) and divergent stagnation regions (unstable focus points). As seen, DNS and TRANS results show qualitatively very similar patterns. The only difference is in the size of the rolls – DNS shows smaller roll patterns but this is to expect due to smaller value of Ra number. Another reason is that the TRANS can per se capture only the very large structure while the smaller ones are filtered out.

In order to provide a further analysis of the spatial organisation of the flow, various vortex identification techniques were applied in parallel to both the DNS and TRANS results. The computed second invariants of the velocity gradient tensor ($I_2 = Q$) are presented in Fig. 9. By taking different positive values of $I_2$, regions with different vortical intensities can be filtered out. A decrease in the values of $I_2$ leads to a more population of the vortical eddies. In parallel to $I_2$, the $\Delta$ approach was applied to the same dataset. Very similar structures were captured with both methods. The same identification techniques were applied for instantaneous TRANS results. As seen, many of the characteristic vortical-eddy shapes observed in DNS field can be recognised in TRANS results too.

### 4.2. High Ra number

As in the previous low Ra case, the characteristic time evolution of the maximum velocity components as well as the overall Nusselt number at hot and cold wall are monitored, Fig. 10. After initial period of time ($0 < \tau^* < 40$) the flow starts to exhibit a convection dominated regime, characterised by a dramatic increase in all velocity components. This is accompanied by a very intensive heat transfer ($40 < \tau^* < 70$).

The streamline distribution show very intensive motion over entire flow domain. The spatial distributions of the second invariant of the velocity gradient tensor ($I_2$) portray the organised structures in the flow. A visual inspection of the streamlines and the corresponding distribution of $I_2$ show that the $I_2$ approach captures well the regions where rotation is present. Very similar pictures are obtained by applying $\Delta$ and $\mathcal{N}_k$ criteria. After $\tau^* = 80$, strong irregularly periodic oscillations of all maximum velocity components are still present, but the overall Nu numbers on both walls reach almost steady values. The number of peaks in the thermal structure becomes smaller at a later stage, but the amplitude

is higher (the peaks almost reach the opposite wall). The motion is very intensive, but shows well organised spatial regions of $I_2$. This confirms the view that the major role of coherent structures is to promote and intensify the momentum and heat transfer.

## 5. Conclusions

Numerical simulations of a Rayleigh–Bénard convection with a conventional single-point turbulence closure demonstrate that the Reynolds-averaged-Navier–Stokes method (RANS), applied in transient mode can well reproduce the mean flow properties, wall heat transfer and second-moment turbulence statistics. Moreover, the computations capture the large scale structure in accord with the DNS and experimental findings. The approach can be regarded as VLES, with a single-point closure playing the role of a 'subgrid scale model'. In comparison with the conventional LES, the model of the unresolved motion (here an algebraic $k-\varepsilon-\overline{\theta^2}$ model) covers a much larger part of turbulence spectrum (in fact almost the complete turbulence, apart from the large coherent structure). This contribution becomes dominant in the near wall region. Because the adopted model of the unresolved motion was already tuned to reproduce near-wall flow properties for a variety of situations (though for near-equilibrium conditions), this model ensures good results also in the present transient RANS (TRANS) approach. The weaknesses of the conventional single-point model, particularly in regard to the convective transport by large structures (modelled usually as gradient diffusion) are removed by time and space resolution of the large structures. The computed mean temperature, its variance, turbulent heat flux and wall heat transfer for Rayleigh Bénard convection over a flat wall in a range of Rayleigh numbers ($10^6$–$10^9$) agree well with available DNS and experimental results. Application of several structure identification methods (second invariant of the velocity gradient tensor, discriminant of the characteristic equation, and kinematic vorticity number) to a parallel analysis of selected TRANS and DNS realisations show a close similarity of the spatial organisation and of the main features of the large coherent structure. This is also confirmed by instantaneous trajectory visualisation.

## Acknowledgements

Authors acknowledge fruitful discussions with Dr Dominique Laurence from DER-LNH of the Electricite de France, during his stay at the Delft University of Technology as visiting scholar of the J.M. Burgerscentrum for Fluid Mechanics. Thanks are also due to Dr G. Grötzbach and Dr M. Wörner, Kernforschungszentrum Karlsruhe, Germany, for providing the DNS realisations. Supercomputing was provided by Stichting Academisch Rekencentrum Amsterdam (SARA), The Netherlands.

## References

Adrian, R.J., Ferreira, R.T.D.S., Boberg, T., 1986. Turbulent thermal convection in wide horizontal fluid layers. Experiments in Fluids 4, 121–141.

Blackburn, H.M., Mansour, N.N., Cantwell, B.J., 1996. Topology of fine-scale motions in turbulent channel flow. J. Fluid Mech 310, 269–292.

Castaing, B., Gunaratne, G., Heslot, F., Kadanoff, L., Libchaber, A., Thomae, S., Wu, X.Z., Zaleski, S., Zanetti, G., 1989. Scaling of hard thermal turbulence in Rayleigh–Bénard convection. J. Fluid Mech 204, 1–30.

Chong, M.S., Perry, A.E., Cantwell, B.J., 1990. A general classification of three-dimensional flow field. Phys. Fluids A 2, 765.

Chong, M.S., Soria, J., Perry, A.E., Chacin, J., Cantwell, B.J., Na, Y., 1998. Turbulence structures of wall-bounded shear flows using DNS data. J. Fluid Mech 357, 225–247.

Chu, T., Goldstein, R.J., 1973. Turbulent natural convection in a horizontal layer of water. J. Fluid Mech 60, 141–159.

Chung, M.K., Yun, H.C., Adrian, R.J., 1992. Scale analysis and wall-layer model for the temperature profile in a turbulent thermal convection. Int. J. Heat Mass Transfer 35 (1), 43–51.

Cortese, T., Balachandar, S., 1993. Vortical nature of thermal plumes in turbulent convection. Phys. Fluids A 5 (12), 3226–3232.

Dol, H.S., Hanjalić, K., Kenjereš, S., 1997. A comparative assessment of the second-moment differential and algebraic models in turbulent natural convection. Int. J. Heat and Fluid Flow 18, 4–14.

Eidson, T.M., 1985. Numerical simulation of the turbulent Rayleigh–Bénard problem using subgrid model. J. Fluid Mech 158, 245–268.

Fitzjarrald, D.E., 1976. An experimental study of turbulent convection in air. J. Fluid Mech. 73, 693–719.

Grötzbach, G., 1982. Direct numerical simulation of laminar and turbulent Bénard convection. J. Fluid Mech 119, 27–53.

Grötzbach, G., 1983. Spatial resolution requirement for direct numerical simulation of Rayleigh–Bénard convection. J. Comput. Phys 49, 241–264.

Hanjalić, K., 1994. Achievements and limitations in modelling and computation of buoyant turbulent flows and heat transfer. Proceedings of the Tenth International Heat Transfer Conference 1, 1–10.

Hunt, J.C.R., Wray, A.A., Moin, P., 1988. Eddies, stream and convergence zones in turbulent flows. Centre for Turbulence Research Report CTR-588, 193.

Ince, N.Z., Launder, B.E., 1989. On the computation of buoyancy-driven turbulent flows in rectangular enclosures. Int. J. Heat Fluid Flow 10, 110–117.

Jeong, J., Hussain, F., 1995. On the identification of a vortex. J. Fluid Mech 285, 69–94.

Kerr, M.R., 1996. Rayleigh number scaling in numerical convection. J. Fluid Mech 310, 139–179.

Kasagi, N., Sumitani, Y., Suzuki, Y., Ilida, O., 1995. Kinematics of the quasi-coherent vortical structure in near-wall turbulence. Int. J. Heat and Fluid Flow 16 (1), 1–10.

Kenjereš, S., Hanjalić, K., 1995. On the prediction of thermal convection in horizontal slender enclosures. In: Proceedings of the Tenth Symposium on Turbulent Shear Flows, Pennsylvania State Univ., USA.

Malkus, W.V.R., 1954. The heat transport and spectrum of thermal turbulence. Proc. Roy. Soc., London A225, 195–212.

Melander, M.V., Hussain, F., 1992. Polarised vorticity dynamics on a vortex column. Phys. Fluids A 5.

Peng, S.H., Davidson, L., 1998. Comparison of subgrid-scale models in LES for turbulent convection flow with heat transfer. In: Second EF Conference in Turbulent Heat Transfer, Manchester, UK.

Perry, A.E., Chong, M.S., 1987. A description of eddying motions and flow patterns using critical point concepts. Ann. Rev. Fluid Mech 19, 125–155.

Priestley, C.H., 1955. Convection from a large horizontal surface. Aust. J. Phys 7, 176–198.

Robinson, S.K., 1991. Coherent motions in the turbulent boundary layer. Annu. Rev. Fluid Mech 23, 601–639.

Sandham, N.D., Kleiser, L., 1992. The late stages of transition to turbulence in channel flow. J. Fluid Mech 245, 319–348.

Siggia, E.D., 1994. High Rayleigh number convection. Annu. Rev. Fluid Mech 26, 137–168.

Threlfall, D.C., 1975. Free convection in low-temperature gaseous helium. J. Fluid Mech 67, 17–28.

Wörner, M., 1994. Direkte Simulation turbulenter Rayleigh-Bénard Konvektion in flüssigem Natrium, Dissertation, Uni. of Karlsruhe, KfK 5228, Kernforschungszentrum Karlsruhe.

Wong, V.C., Lilly, D.K., 1994. A comparison of two dynamical subgrid closure methods for turbulent thermal convection. Phys. Fluids 6 (2), 1016–1023.

Wu, X.Z., Libchaber, A., 1992. Scaling relations in thermal turbulence: The aspect ratio dependence. Phys. Rev. A 45 (2), 842–845.